Alexandria Engineering Journal (2023) 75, 297–312

HOSTED BY

Alexandria University

Alexandria Engineering Journal

www.elsevier.com/locate/aej
www.sciencedirect.com

ORIGINAL ARTICLE

Dual solutions of convective rotating flow of three-dimensional hybrid nanofluid across the linear stretching/shrinking sheet

Adnan Asghar [a], **Narcisa Vrinceanu** [b,*], **Teh Yuan Ying** [a], **Liaquat Ali Lund** [c], **Zahir Shah** [d,*], **Vineet Tirth** [e,f]

[a] *School of Quantitative Sciences, UUM College of Arts & Sciences, Universiti Utara Malaysia, UUM Sintok, Kedah Darul Aman, Malaysia*
[b] *Faculty of Engineering, Department of Industrial Machines and Equipments, "Lucian Blaga" University of Sibiu, 10 Victoriei Boulevard, Romania*
[c] *KCAET Khairpur Mir's, Sindh Agriculture University, Tandojam Sindh 70060, Pakistan*
[d] *Department of Mathematical Sciences, University of Lakki Marwat, Lakki Marwat 28420, Khyber Pakhtunkhwa Pakistan*
[e] *Mechanical Engineering Department, College of Engineering, King Khalid University, Abha 61421, Asir, Saudi Arabia*
[f] *Research Center for Advanced Materials Science (RCAMS), King Khalid University, Guraiger, Abha 61413, Asir, Saudi Arabia*

Received 9 March 2023; revised 10 May 2023; accepted 28 May 2023

KEYWORDS

Three dimensional (3-D);
Rotational parameter;
Viscous dissipation;
Biot number;
Dual solution

Abstract A numerical study was carried out on dual solutions of rotating stretching/shrinking surfaces to explore the influence of convective boundary conditions, viscous dissipation, thermal radiation, and heat sources/sinks on 3-D hybrid nanofluid flow. Hybrid nanofluids have great potential for a variety of applications due to their unique properties and versatility. It is improved the effectiveness of heat transfer rates. The main objective of this study is to investigate the influence that certain parameters on the temperature and velocities profiles against the parameters, including the volume fraction of copper, suction effect, viscous dissipation, thermal radiation, Biot number and rotating parameter. Further, the impact of the suction effect and shrinking sheet on reduced heat transfer and skin friction is also considered against the volume fraction of copper. The nonlinear partial differential equations are transformed into a collection of ordinary differential equations by including linear similarity variables. The generated combination of higher order nonlinear ODEs is solved via a boundary value algorithm called bvp4c, which executes on the MATLAB computing tool. The findings confirmed the existence of two branches (dual solution) with varied quantities of copper volume fraction according to the shrinking surface and suction effect. Additionally, as the Biot number, Eckert number, thermal radiation, and copper volume fraction all increase in strength, the rate at which heat flows in both solutions also increases. However, the heat transfer rate declined as increased the suction effect. Besides, when a positive and negative increment is applied to the rotational parameter, both solutions suffer an increase in both velocities. In

* Corresponding authors.
E-mail addresses: vrinceanu.narcisai@ulbsibiu.ro (N. Vrinceanu), Zahir@ulm.edu.pk (Z. Shah).
Peer review under responsibility of Faculty of Engineering, Alexandria University.

https://doi.org/10.1016/j.aej.2023.05.089
1110-0168 © 2023 THE AUTHORS. Published by Elsevier BV on behalf of Faculty of Engineering, Alexandria University.
This is an open access article under the CC BY-NC-ND license (http://creativecommons.org/licenses/by-nc-nd/4.0/).

Nomenclature

C_{fx}	Skin friction coefficient along x-axis
C_{fy}	Skin friction coefficient along y-axis
Nu_x	Local Nusselt number
(ρc_p)	Heat capacity (J/m^3K)
k	Thermal conductivity (W/mK)
a	Positive constant
T_∞	Ambient temperature (K)
T	Fluid temperature(K)
T_0	Characteristic temperature (K)
l	Characteristic length (m)
U_w	Surface velocity
w_w	Mass flux velocity (m/s)
S	Suction parameter
λ	Stretching/shrinking parameter
q_r	Radiative heat flux
q	Heat source/sink coefficient
Q	Heat source/sink parameter
Ec	Viscous dissipation parameter
Bi	Biot number parameter
T_f	Heats the sheet's bottom
h_f	Heat transfer coefficient
Pr	Prandtl number
Rd	Thermal radiation
Re_x	Local Reynolds number
2-D	Two dimensional
3-D	Three dimensional
u, v, w	Velocity components in x, y, z axes (m/s)
x, y, z	Cartesian coordinate axes

Greek Symbols

k^1	Mean absorption coefficient
σ_1	Stefan-Boltzmann constant
η	Similarity variable
θ	Dimensionless temperature
ω	Rotational parameter
ν_f	Kinematic viscosity (m^2/s)
ρ	Density (kg/m^3)
μ	Dynamic viscosity (Kg/ms)
$\varphi_{Al_2O_3}$	Solid volume fraction for Alumina (Al_2O_3)
φ_{Cu}	Solid volume fraction for copper (Cu)

Subscripts

f	Base fluid
nf	Nanofluid
hnf	Hybrid nanofluid
S_1	Solid nanoparticle for Alumina (Al_2O_3)
S_2	Solid nanoparticle for copper (Cu)
∞	Far field conditions/ambient
c	Critical
w	Surface condition

Superscript

$\prime$	Differentiation with respect to η

summary, unique solutions are obtained $S < S_{ci}$ for suction effect and $\lambda < \lambda_{ci}$ for the shrinking region. The outcomes came to the conclusion that hybrid nanofluid has a faster rate of transferring heat than standard nanofluid offers.

© 2023 THE AUTHORS. Published by Elsevier BV on behalf of Faculty of Engineering, Alexandria University. This is an open access article under the CC BY-NC-ND license (http://creativecommons.org/licenses/by-nc-nd/4.0/).

1. Introduction

Over the course of the last few years, research into a novel approach to the problem of boundary layer flow that focuses on the enhancement of the transfer of heat in hybrid nanofluids has been examined. In response to the growing trend for rates of heat transfer from various facets of the industry, scientists have tried including a large number of solid nanoparticles through a variety of base fluids. It is notable to mention that the mathematical models of nanofluids that were presented by Buongiorno [1] and Tiwari and Das [2] were utilized quite frequently in the field of fluid dynamics. The thermophoresis processes and Brownian motion impacts on laminar fluid flow are taken into consideration by the nanofluid model developed by Buongiorno. In the meantime, the Tiwari-Das model investigates the behaviour of a nanofluid in consideration of the nanoparticles' solid volume fractions. However, with a goal to enhance the thermophysical characteristics of conventional nanofluid, a new type of nanofluid identified as a "hybrid nanofluid" was developed. After that, Devi and Devi [3] considerably improved thermal characteristics may be achieved by mixing a solid nanoparticle in a tiny nanotube/quantity by an oxide or suspensions of solid particles in a base fluid. The expression "hybrid nanofluid" refers to a type of normal fluid, such as (vegetable oil, glycol, water, engine oil, ethylene, kerosene, and paraffin oil) that typically contains more than one solid nanoparticle. Hybrid nanofluids have been employed in various heat transport appliances, such as heat tray converters, microchannels, heat valves, funnel cooling systems, air conditioning units, small channel passive heat sinks, etc., as described by Asghar et al. [4]. Waini et al. [5] looked into radiation's impacts on a hybrid nanofluid with a nonlinear stretched/shrunk layer. Besides that, Waini et al. [6] analyzed the consequences of 2-D flow by heat transport across a stretched/diminishing sheet. Numerous researchers have thoroughly investigated the underlying mechanisms of various suggested models on boundary layer flow with different parameters for nanofluids and hybrid nanofluids [7–32].

Several industries, such as manufacturing techniques (e.g., spinning equipment, centrifugal purification method, digital

recording equipment, etc.), make use of rotational flow. Hayat and Nadeem [33] addressed the 3-D flow while considering the existence of chemical processes, heat sink factor, and thermal radiation parameters. They observed that a hybrid nanofluid had a significantly higher heat transfer rate than a conventional fluid. In addition, they discovered that an improvement in the rotation parameter causes augmentation in the concentration profile. Moreover, Hayat et al. [34] examined the power of radiation and slip conditions on a 3-D rotational flow of a hybrid nanofluid. They demonstrated that raising the rotational parameters enhanced the temperature profile. In a later study, Anuar et al. [35] analyzed the consequences of radiation on the rotating 3-D steady flow for stretching and shrinking layer. In addition, Ying and Asghar [36] explored the hybrid nanofluid through the occurrence of magnetic field and Joule heating in a 3-D flow that was rotational while stretching and shrinking sheet. Several researchers have studied the effects of rotational stretching/shrinking sheet for hybrid nanofluids using various theoretical frameworks [37–39].

It is hard to overlook the fact that thermal radiation has a substantial effect on exceptionally high-temperature applications. In many industrial operations, temperatures may reach very high levels, making thermal radiation sensitivity an absolute must for developing appropriate machinery. It also has abundant real-world applications in the trade sector, such as in the production of glass and the design of furnaces, and in the aerospace industry, where it is used in the creation of solar radiations, spacecraft, launch systems, combustion engines and boat steam turbines (Khan et al. [40]). A 2-D unsteady flow heat transport study of a hybrid nanofluid along a stretched sheet was reported by Sreedevi et al. [41]. Recently, using computational methods, Dero et al. [42] evaluated the crossflow of hybrid nanofluid by the impact of radiation. These researches contain some recent articles on thermal radiation [43–45].

The heat source and heat sink are also critical components in controlling heat transmission. Many industrial operations, such as chilling nuclear power stations, hydrothermal sources, and energy absorption, highlight the importance of understanding the presence and impacts of heat sources and sinks (Zainal et al. [46]). In the existence of heat absorption/generation, radiation and chemical processes, Hayat and Nadeem [33] analyzed the steady flow of 3-D hybrid nanofluid. Furthermore, the steady flow over an exponential stretched and contracting permeable layer was investigated in 2-D by Wahid et al. [47] under the slip circumstances and heat source effect. As aforementioned, Zainal et al. [46] looked at how the heat source/sink affected the bidirectionally stretched/diminishing layer for a hybrid nanofluid. There have been many studies on heat sources and sinks, as well as [48–49].

Viscous dissipation is the process by which work done under viscous forces changes the kinetic energy of a fluid into thermal energy. When it comes to energy dissipation caused by viscous heating, the huge velocity gradients inside the boundary layer have a significant bearing on the situation. Kishore et al. [50] assert that the viscous heat dissipation in the normal convection flow performs a vital part in geophysical fluxes, particularly industrial processes, which are often described through the Eckert number parameter. The Eckert number is an expression of viscous dissipation that may be defined as the kinetic energy ratio flows to heat conversion enthalpy driving intensity. Gebhart [51] investigated how viscous dissipation affected the temperature in a naturally occurring convection flow for the first time. Moreover, Zainal et al. [52] explored the impact of magnetic field and viscous dissipation in 2-D stretched/diminishing sheet. Recently Wahid et al. [53] explored the 3-D steady flow through viscous dissipation, Joule heating, and slip factors. Some more studies on viscous dissipation can be seen in this literature [54–55].

Boundary conditions are constraints that must be satisfied at the edges of a physical system, such as a solid, a fluid, or an electromagnetic field. These conditions play a crucial role in determining the behavior of the system and its interactions with its surroundings. Physically, boundary conditions can be understood as the specific conditions that exist at the interfaces between different materials or regions of space. For example, if we consider the behavior of a fluid flowing through a pipe, the boundary conditions at the walls of the pipe may specify the velocity or pressure of the fluid at those points, or they may specify that the fluid cannot penetrate the wall or surface. Convective boundary conditions are also significant in studying boundary layer. It is also referred to as the Robin condition. Substantially, it may be defined as a situation in which heat convection and conduction at the layer are equal. The nuclear power plant, oxygenation, laser treatment, gas turbines, sanitary fluid transportation, hemodialysis, and material drying are examples of practical applications for convective boundary conditions (Sayed et al. [56]). Aziz [57] first reported using convective boundary conditions while analyzing the Blasius flow. Furthermore, Devi and Devi [58] analyzed the 3-D flow over a stretching layer with the influence of Newtonian heating and convective boundary conditions. Aly and Pop [59] analyzed the 2-D over a stretch and diminishing sheet utilizing suction and convective boundaries. Moreover, Khashi et al. [60] studied steady hybrid nanofluid flow passes stretching/shrinking layer by convective boundary and velocity slip conditions. Additionally, several studies explored the influences of the convective boundary condition with different consideration models in hybrid nanofluids [61–63].

Currently, most research on incorporated hybrid nanofluids with convective boundary conditions, viscous dissipation, thermal radiation and heat sources/sink impacts is limited to steady flow in two dimensions (2-D) (refer to Sreedevi et al. [41], Wahid et al. [47], Zainal et al. [52], Waini et al. [62]). However, according to the research that came before it, conducting a literature review reveals that it is essential to investigate problems such as three-dimensional flow since this context enables applications that are both more complete and more real to life in the real world. Khashi et al. [60] investigated three-dimensional (3-D) hybrid nanofluid flow and heat transfer with stretching/shrinking surface under convective and velocity slip conditions but without accounting for radiation, viscous dissipation, heat source/sink, and rotational flow parameter. However, the proposed problem intends to cover the gaps identified by Khashi et al. [60] by examining the effect of rotational parameters, radiation, viscous dissipation, heat source/sink, and convective boundary conditions employing the Tiwari and Das model (refer to Tiwari and Das [2]). Therefore, a novel physical framework of three-dimensional (3-D) radiative rotating hybrid nanofluid flow on stretching/shrinking surfaces by the effect of convective boundary conditions, heat source/sink, radiation, and viscous dissipation was formed for this investigation. The existing research objectives are to explore the velocity and temperature profiles are inves-

tigated for a variety of solid volume fraction copper values, as well as suction, viscous dissipation, radiation, Biot number, and rotational parameter. In addition, this research looks at the way the influence of solid volume fraction copper under suction and stretching/shrinking surface affects the variability of reduced skin friction and reduced heat transfer.

Copper (Cu) and Alumina (Al_2O_3) nanoparticles are employed in this study's hybrid nanofluid to achieve excellent convective heat transfer efficiency. Copper (Cu) nanoparticles have high thermal conductivity, which means they are very effective at transferring heat. This makes them useful for applications such as cooling electronic devices or heat exchangers. In a hybrid nanofluid, the copper nanoparticles can improve the thermal conductivity of the fluid, making it more efficient at transferring heat. Alumina (Al_2O_3) nanoparticles, on the other hand, have high mechanical strength and wear resistance. This makes them useful for applications such as coatings in structural materials. In a hybrid nanofluid, the alumina nanoparticles can improve the mechanical properties of the fluid, making it stronger and more resistant to wear. By combining alumina (Al_2O_3) and copper (Cu) nanoparticles in a hybrid nanofluid, the resulting fluid can have improved thermal and mechanical properties, making it useful for a wide range of applications. For the aim of making comparisons, the current numerical outcomes are weighed against the outcomes of prior research. To the best of our understanding, this model is unique and novel, and a search of the relevant literature turned up no articles that were relevant to it.

2. Mathematical formulation

Fig. 1 illustrates a 3-D hybrid nanofluid steady flow by stretching and shrinking sheets. These sheets have Cartesian coordinates, with the x- and y-axes being expressed in the $z = 0$ plane. At $z \geq 0$, half of the region is taken up by this fluid. The physical model is described by the mathematical governing equations using the concepts of incompressible, Newtonian, and laminar flow. The following assumptions are made about the sheet at $z = 0$.

i. The surface velocity $U_w = ax$ deemed to be stretching/shrinking in the x-direction.
ii. The system rotates in a direction that is normal to the surface z-axis at a constant velocity.
iii. q_r is radiation along the z-axis, and
iv. $q$is the coefficient of heat source/sink also deemed in this study.

The hybrid nanofluid's surface is constant. Additionally, it is presumed that a hot fluid with a uniform temperature T_f heats the sheet's bottom through convection. Besides, the coefficient of heat transfer is h_f. It can be seen in Fig. 1 that both the fluid phases and the nanoparticles are presumed to be in a condition of thermal equilibrium. Because of their exceptionally small size and consistent shape, the slip velocity between phases may be neglected in their existence.

The governing equations for a hybrid nanofluid are as described: (Anuar et al. [35]; Khashi et al. [60])

$$\frac{\partial u}{\partial x}+\frac{\partial v}{\partial y}+\frac{\partial w}{\partial z}=0 \tag{1}$$

$$u\frac{\partial u}{\partial x}+v\frac{\partial u}{\partial y}+w\frac{\partial u}{\partial z}-2\Omega v=\frac{\mu_{hnf}}{\rho_{hnf}}\frac{\partial^2 u}{\partial z^2} \tag{2}$$

$$u\frac{\partial v}{\partial x}+v\frac{\partial v}{\partial y}+w\frac{\partial v}{\partial z}+2\Omega u=\frac{\mu_{hnf}}{\rho_{hnf}}\frac{\partial^2 v}{\partial z^2} \tag{3}$$

$$u\frac{\partial T}{\partial x}+v\frac{\partial T}{\partial y}+w\frac{\partial T}{\partial z}=\frac{k_{hnf}}{(\rho c_p)_{hnf}}\frac{\partial^2 T}{\partial z^2}-\frac{1}{(\rho c_p)_{hnf}}\frac{\partial q_r}{\partial z}+\frac{\mu_{hnf}}{(\rho c_p)_{hnf}}\left(\frac{\partial u}{\partial z}\right)^2+\frac{q}{(\rho c_p)_{hnf}}(T-T_\infty). \tag{4}$$

With boundary conditions (Khashi et al. [60]; Anuar et al. [35]).

$$u=\lambda U_w, v=0, w=w_w, -k_{hnf}\frac{\partial T}{\partial z}=h_f(T_f-T), \text{ as } z=0, \tag{5}$$

$$u\to 0, v\to 0, T\to T_\infty \text{as} z\to\infty \tag{6}$$

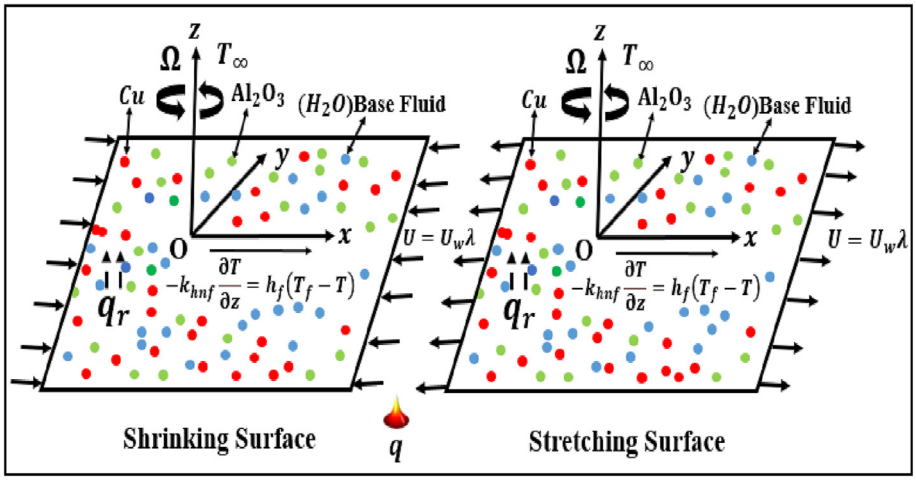


Fig. 1 A geometrically stretching and shrinking surface model.

Table 1 The hybrid nanofluid characteristics.

Names	Properties
Dynamic Viscosity	$\mu_{hnf} = \frac{\mu_f}{(1-\varphi_{Al_2O_3})^{2.5}(1-\varphi_{Cu})^{2.5}}$
Density	$\rho_{hnf} = (1-\varphi_{Cu})\left[(1-\varphi_{Al_2O_3})\rho_f + \varphi_{Al_2O_3}\rho_{Al_2O_3}\right] + \varphi_{Cu}\rho_{Cu}$
Heat capacity	$(\rho c_p)_{hnf} = (1-\varphi_{Cu})\left[(1-\varphi_{Al_2O_3})(\rho c_p)_f + \varphi_{Al_2O_3}(\rho c_p)_{Al_2O_3}\right] + \varphi_{Cu}(\rho c_p)_{Cu}$
Thermal conductivity	$k_{hnf} = \frac{k_{Cu}+2k_{nf}-2\varphi_{Cu}(k_{nf}-k_{Cu})}{k_{Cu}+2k_{nf}+\varphi_{Cu}(k_{nf}-k_{Cu})} \times (k_{nf})$ where $k_{nf} = \frac{k_{Al_2O_3}+2k_f-2\varphi_{Al_2O_3}(k_f-k_{Al_2O_3})}{k_{Al_2O_3}+2k_f+\varphi_{Al_2O_3}(k_f-k_{Al_2O_3})} \times (k_f)$

The velocities elements u, v, and w, by the x-axis, y-axis, and z-axis, respectively, for hybrid nanofluid. λ demonstrates the parameter's constant stretching and shrinking, besides when $\lambda = 0$, $\lambda > 0$, and $\lambda < 0$ are static, stretching and shrinking sheet. T_∞ represents ambient temperature and the fluid's temperature is T. q_r represented the radiative heat flux (Anuar et al. [35]):

$$q_r = -\frac{4\sigma_1}{3k^1}\frac{\partial T^4}{\partial y} \tag{7}$$

σ_1 and k^1 correspond to the Stefan-Boltzmann constant and the mean absorption coefficient, respectively. By ignoring the higher-order conditions and developing T^4 through a Taylor series about T_∞. Further transforms $T^4 \cong 4\ T_\infty^3\ T - 3T_\infty^4$. Therefore, as a consequence, the energy Equation (4) be converted into the following,

$$u\frac{\partial T}{\partial x} + v\frac{\partial T}{\partial y} + w\frac{\partial T}{\partial z} = \left[\frac{k_{hnf}}{(\rho c_p)_{hnf}} + \frac{16\sigma_1 T_\infty^3}{3k^1(\rho c_p)_{hnf}}\right]\frac{\partial^2 T}{\partial z^2} + \frac{\mu_{hnf}}{(\rho c_p)_{hnf}}\left(\frac{\partial u}{\partial z}\right)^2 + \frac{q}{(\rho c_p)_{hnf}}(T - T_\infty). \tag{8}$$

The stated equations were determined using hybrid nanofluid characteristics, as shown in Table 1. Besides, Table 2 shows the characteristics of the solid nanoparticles and normal fluid (H_2O). Further $k_{hnf}, (\rho c_p)_{hnf}, \rho_{hnf}$, and$\mu_{hnf}$ which indicates the thermal conductivity, heat capacity, density, and dynamic viscosity for hybrid nanofluid correspondingly. Copper (Cu) and alumina (Al_2O_3) solid volume fractions are signified by φ_{Cu} and $\varphi_{Al_2O_3}$ correspondingly. The hybrid nanofluid, nanofluid, fluid, solid particle S_1, and solid particle S_2 subscript denoted hnf, nf, f,Al_2O_3 and Cu, correspondingly.

Table 2 The characteristics of solid nanoparticles and normal fluid (H_2O).

Fluids	$k\ (W/m\ K)$	$\rho(kg/m^3)$	$c_p(J/kg\ K)$	Pr
Alumina (Al_2O_3)	40	3970	765	–
Water (H_2O)	0.613	997.1	4179	6.2
Copper (Cu)	400	8933	385	–

In this case, the similarity variables are described below; (Khashi et al. [60]; Anuar et al. [35]).

$$u = axf'(\eta),\ v = axg(\eta),\ w = -\sqrt{av_f}f(\eta),$$
$$\theta(\eta) = \frac{T - T_\infty}{T_f - T_\infty},\ \eta = z\sqrt{\frac{a}{v_f}} \tag{9}$$

Here v_f kinematic viscosity, and $a$is a positive constant of the fluid. While $w_w = -\sqrt{av_f}S$, S stands for the injection/suction parameter, such as $S > 0$ for suction and when using $S < 0$ for injection.

Equation (1) is identically fulfilled, and Equation (9) is substitute into Equations (2–4). Then, The Eqs. (2)–(4) were converted into the ODEs equations shown below.

$$\frac{A}{A^*}f''' - (f')^2 + f''f + 2\omega g = 0 \tag{10}$$

$$\frac{A}{A^*}g'' + g'f - gf' - 2\omega f\prime = 0 \tag{11}$$

$$\frac{1}{PrB}\left\{B^* + \frac{4Rd}{3}\right\}\theta'' + \theta' f - 2\theta f' + \frac{A}{B}Ec(f'')^2 + \frac{1}{B}Q\theta = 0. \tag{12}$$

where $\mu_{hnf}/\mu_f = A$, $\rho_{hnf}/\rho_f = A^*$, $(\rho c_p)_{hnf}/(\rho c_p)_f = B$, and $k_{hnf}/k_f = B^*$,

Depending on the boundary conditions:

$$f(0) = S, g(0) = 0, f'(0) = \lambda, -B^* * \theta'(0) = Bi[1 - \theta(0)] \tag{13}$$

$$f'(\eta) \to 0, \theta(\eta) \to 0, g(\eta) \to 0 \text{as} \eta \to \infty \tag{14}$$

While ω rotation parameter, Q is heat source/sink parameter, $Ec$is Eckert number for viscous dissipation parameter,q_r radiative heat flux, Pr Prandtl number, and Bishows the Biot number paramter, which are described in Equation (15):

$$\omega = \frac{\Omega}{a},\ Q = \frac{q}{a(\rho c_p)_f},\ Ec = \frac{a^2 l^2}{T_0(c_p)_f},$$
$$q_r = -\frac{4\sigma_1}{3k^1}\frac{\partial T^4}{\partial y},\ Pr = \frac{(\mu c_p)_f}{k_f},\ \text{and}\ Bi = \frac{h_f}{k_f}\sqrt{\frac{v_f}{a}}. \tag{15}$$

The skin friction coefficients C_{fx} and C_{fy}, show that x- and y-axes, respectively, and local Nusselt number Nu_x, which is identified as:

$$C_{fx} = \frac{A}{U_w^2}\left(\frac{\partial u}{\partial z}\right)_{z=0}, C_{fy} = \frac{A}{U_w^2}\left(\frac{\partial v}{\partial z}\right)_{z=0}$$

$$Nu_x = \frac{x}{k_f(T_f - T_\infty)}\left[-k_{hnf}\left(\frac{\partial T}{\partial z}\right)_{z=0} + q_r|_{z=0}\right] \tag{16}$$

By using Equations (9) and (16), it is obtained.

$$\sqrt{Re_x}C_{fx} = A * f''(0),\ \sqrt{Re_x}C_{fy} = A * g'(0),$$
$$\frac{Nu_x}{\sqrt{Re_x}} = -\left[B^* + \frac{4}{3}Rd\right]\theta'(0) \tag{17}$$

Here $Re_x = \frac{U_w x}{\nu_f}$ is local Reynolds number.

3. Numerical method

The higher-order nonlinear ordinary differential equations depicted in Equations (10–12) through the boundary conditions (13) and (14) are determined numerically utilizing the Bvp4c algorithm, which commutes on the Matlab program. The Bvp4c algorithm is a finite differences system that applies the 3-stages Lobatto IIIA implicit Runge Kutta technique and returns numerical results of fourth order correctness (Hale [64]). In order to include the Bvp4c algorithm in our physical model, we proceeded with the following procedures.

STEP 1: Different new variables are proposed for the equations of higher-order nonlinear ODEs in Equations (10)-(12):

$$f = \epsilon_1, f' = \epsilon_2, f'' = \epsilon_3, g = \epsilon_4, g' = \epsilon_5, \theta = \epsilon_6, \theta\prime = \epsilon_7 \tag{18}$$

STEP 2: Reduces the equations of higher-order nonlinear ordinary differential equations in Equation (10)-(12) to an equation of first-order nonlinear ordinary differential equations applying the different new variables into Equation (18):

$$f' = \epsilon_2$$
$$f'' = \epsilon_3$$
$$f''' = \left((\epsilon_2)^2 - \epsilon_3\epsilon_1 - 2\omega\epsilon_4\right)\frac{A^*}{A}$$
$$g' = \epsilon_5 \tag{19}$$
$$g'' = (\epsilon_4\epsilon_2 - \epsilon_5\epsilon_1 + 2\omega\epsilon_2)\frac{A^*}{A}$$
$$\theta' = \epsilon_7$$
$$\theta'' = \left(2\epsilon_6\epsilon_2 - \epsilon_7\epsilon_1 - \frac{A}{B}Ec * (\epsilon_3)^2 - \frac{1}{B}Q*\epsilon_6\right)\frac{PrB}{B^*}$$

STEP 3: Describe the boundaries (13) and (14) in the context of the additional different new variables that have been introduced in Equation (18):

$$(\epsilon_1)_{a^*} = S,\ (\epsilon_4)_{a^*} = 0,\ (\epsilon_2)_{a^*} = \lambda,\ -B^* * (\epsilon_7)_{a^*}$$
$$= Bi[1 - (\epsilon_6)_{a^*}],\ (\epsilon_2)_{b^*} = 0,\ (\epsilon_6)_{b^*} = 0,\ (\epsilon_4)_{b^*} = 0 \tag{20}$$

It is important to notice that the location of the surface at $\eta = 0$ is indicated by the subscript 'a^*' whereas the subscript 'b^*' designates the distance from the surface for a particular quantity of η. In this research, we set this position at $\eta = 14$. Get dual solutions by giving the Bvp4c algorithm two different beginning estimates one at a time. It is possible to get at the first answer using initial predictions that are more open-ended. However, this is not always the case when trying to arrive at a second solution. This procedure is repetitive over and over again until the numerical solutions are able to fulfil the boundary criteria at infinity (i.e. Equation (14) asymptotically.

4. Result and discussion

The dual solutions have been accomplished in Figs. 2-18 by utilizing alternative initial estimations for $f\prime\prime(0)$, $g'(0)$and $-\theta\prime(0)$, which led to the finding that the boundary condition was met $\eta \to \infty$ asymptotically by both velocities profiles and temperature profile. Before beginning to talk about the findings of the recent research, we first verified the programming of a numerical approach to ensure that the code on our computer is operating correctly, initially to verify the algorithm of a numerical method in this research, $f''(0)$ and $g'(0)$ for viscous fluid as $\varphi_{Al_2O_3} = \varphi_{Cu} = S = Q = Rd = Ec = Bi = 0,\ Pr = 6.2$ is matched through outcomes declared by Nazar et al. [65] and Mustafa et al. [66] as in Table 3 for $\lambda = 1$. The conclusions are in line as well as those of other research, and there is a considerable amount of supporting data to back up their validity.

The suction S effect for several amounts by variation values of $f''(0), g'(0)$ and $-\theta'(0)$ through solid volume fraction copper $\varphi_{Cu}$are presented in Figs. 2-4 by the occurrence of distinct parameters quantity, such as $\varphi_{Al_2O_3} = 0.01, Pr = 6.2, \lambda = -1,$ $\omega = Q = 0.01, Rd = Ec = 0.1$and $Bi = 0.1$. The ranges of φ_{Cu} is 0.03 to 0.07 are considered in this study. According to the recommendations provided by Tiwari and Das [2], the values that were chosen for solid nanoparticles φ_{Cu} in Figs. 2-4 fall within the ranges of values that are $0 \le \varphi_{Cu} \ge 0.2$, this range satisfied the boundary condition $\eta \to \infty$ asymptotically and obtained dual solutions. The critical point at the suction effect is shown by the notation S_{ci} when $i = 1, 2, 3$, and it is at this point that both solutions collide with one another. It is demonstrable that when $S < S_{ci}$ no solutions happen, and a non-unique solution exists when $S \ge S_{ci}$. Besides, the value ofS_{ci} = 1.8050, 1.8024, and 1.7490 are correspondingly critical points of $\varphi_{Cu} = 0.03, 0.05,$ and 0.07, respectively. It also is important to disclose at this point that when $\varphi_{Cu} = 0.03$, it is Al_2O_3 /Cu water-based hybrid nanofluid and $S_{c1} = 1.8050$, later 5% of φ_{Cu} is included and made $S_{c2} = 1.8024$. Besides, the value of $S_{c3} = 1.7490$ appeared to grow as 7% of φ_{Cu} is included in fluid. In Fig. 2, the first and second solutions of $f''(0)$ increased when values of φ_{Cu} augmented. Besides, in Fig. 3, the first solution declined, and the second solution of $g\prime(0)$ is enhanced as upsurged the quantity of φ_{Cu}. As demonstrated in Fig. 4, the quantity of φ_{Cu} is a grow, the amount of $-\theta\prime(0)$ as well dropped in both solutions. Physically outcomes show that the boundary layer separation expands as the amount of φ_{Cu} improved. The higher quantity φ_{Cu} would enhance the fluid's velocity, resulting in more friction owing to the fast movement and interaction of the solid nanoparticles. Khashi et al. [60] obtained similar results for $f''(0)$ and $-\theta\prime(0)$.

Figs. 5-7 demonstrate against varying values of solid volume fraction $\varphi_{Cu} = 0.02, 0.05,$ and 0.08 for $(f\prime\prime(0),\ g\prime(0))$, and $-\theta\prime(0)$ with the existence of $\varphi_{Al_2O_3} = 0.01, Pr = 6.2,$ $S = 2.5, \omega = Q = 0.01, Rd = Ec = 0.1$and $Bi = 0.1$ against stretching/shrinking parameter λ. We are able to comprehend that the existence of non-unique solutions is noticeable when it comes to $\lambda \le -1.5$ shrinking sheet. The critical points at which

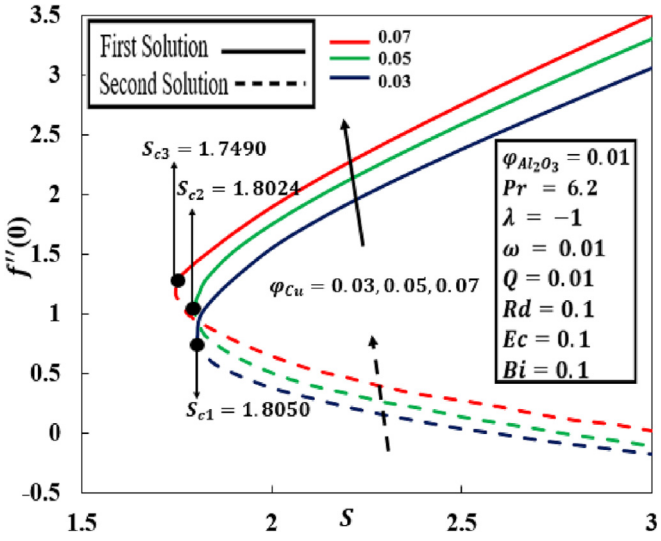


Fig. 2 Behaviour of φ_{Cu} on $f\prime\prime(0)$ for S.

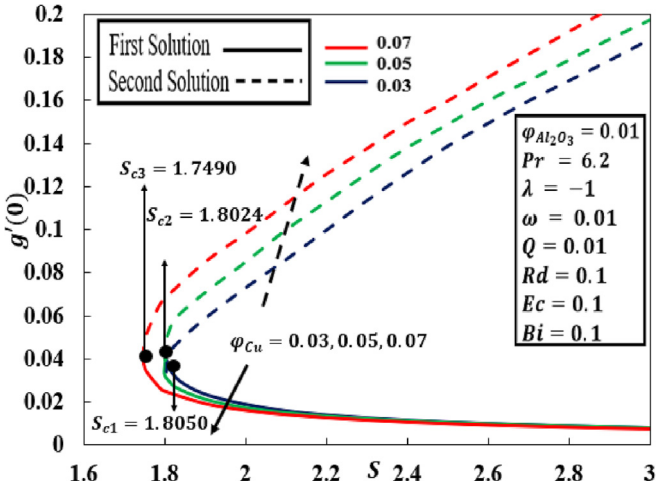


Fig. 3 Behaviour of φ_{Cu} on $g\prime(0)$ for.S.

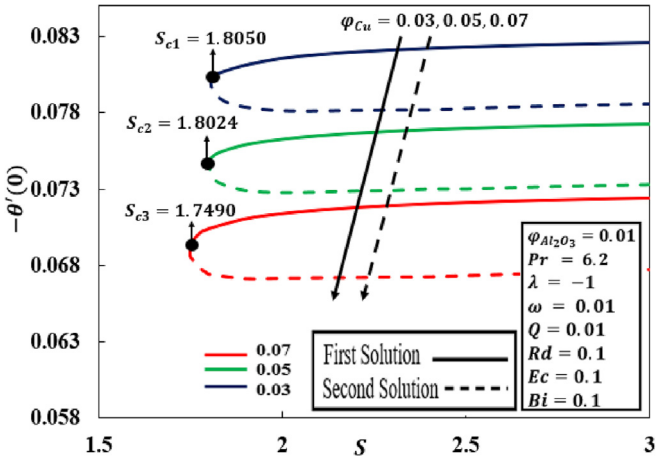


Fig. 4 Behaviour of φ_{Cu} on $-\theta\prime(0)$ for.S.

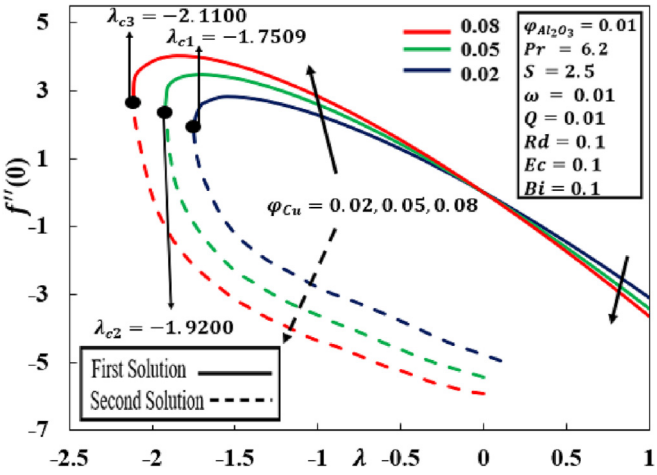


Fig. 5 Behaviour of φ_{Cu} on $f\prime\prime(0)$ for.λ.

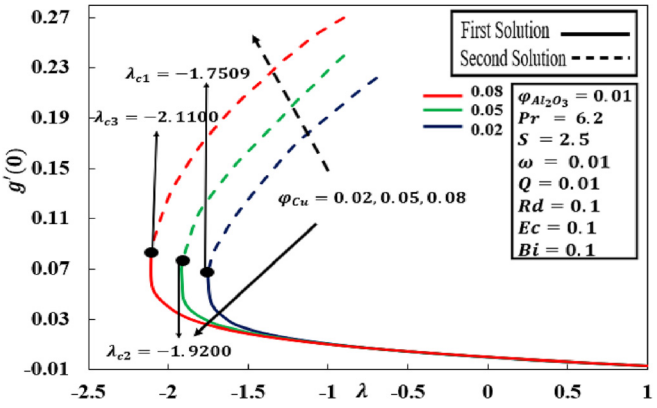


Fig. 6 Behaviour of φ_{Cu} on $g\prime(0)$ forλ.

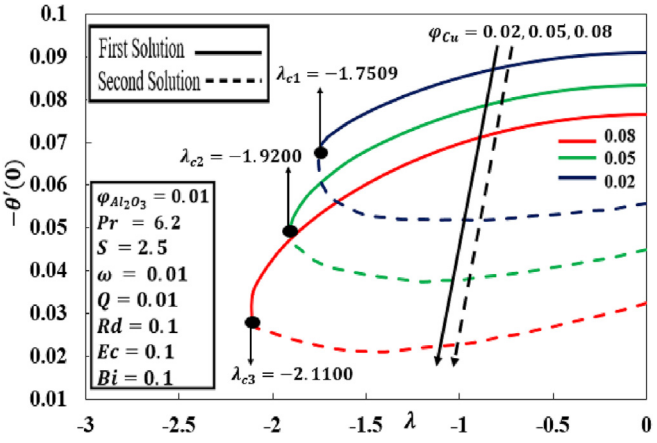


Fig. 7 Behaviour of φ_{Cu} on $-\theta\prime(0)$ for λ.

both solutions converge are denoted by the expression λ_{ci}, $i = 1, 2, 3$, and it is located on the shrinking sheet. It revealed that the dual behaviour exists as $\lambda \geq \lambda_{ci}$ and no solution appears as $\lambda < \lambda_{ci}$, a unique solution is discovered as $\lambda > -1.5$. Since these critical quantities are exceeded, the estimate for the boundary layer can no longer be defended. Additionally, the quantity of $\lambda_{c1} = -1.7509, \lambda_{c2} = -1.9200$ and $\lambda_{c3} = -2.1100$ are the equivalent critical points of $\varphi_{Cu} = 0.02, 0.05,$and 0.08 correspondingly. Fig. 5 indicates that in the first solution, the behaviour of $f\prime\prime(0)$ boosted after $\lambda \leq 0$ and dropped as $\lambda > 0$, but the second solution declined subsequently the augmentation of φ_{Cu}. This occurs due to a

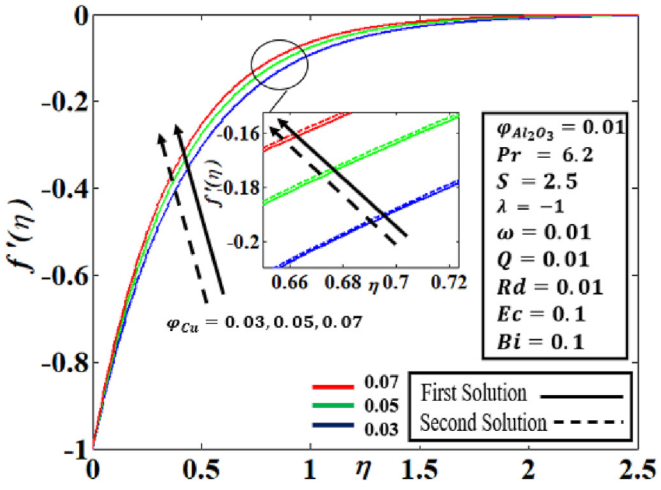


Fig. 8 $f\prime(\eta)$ profile for distinctφ_{Cu}.

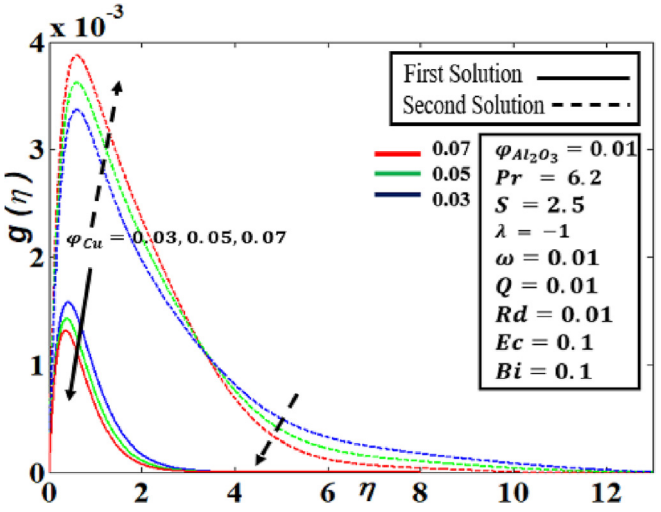


Fig. 9 $g(\eta)$ profile for differentφ_{Cu}.

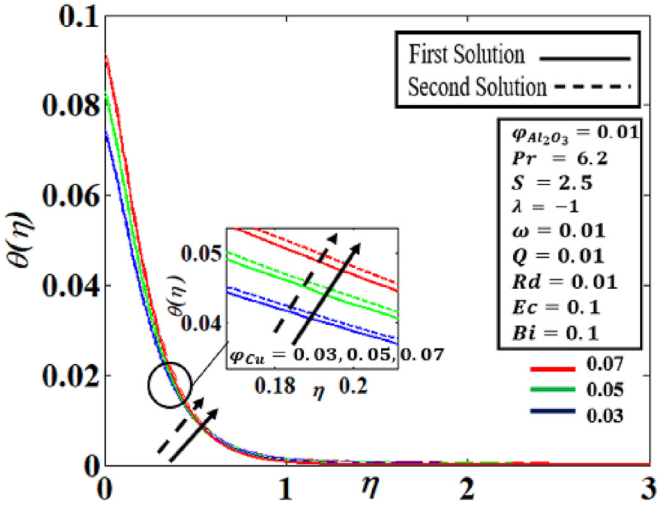


Fig. 10 $\theta(\eta)$ profile for distinctφ_{Cu}.

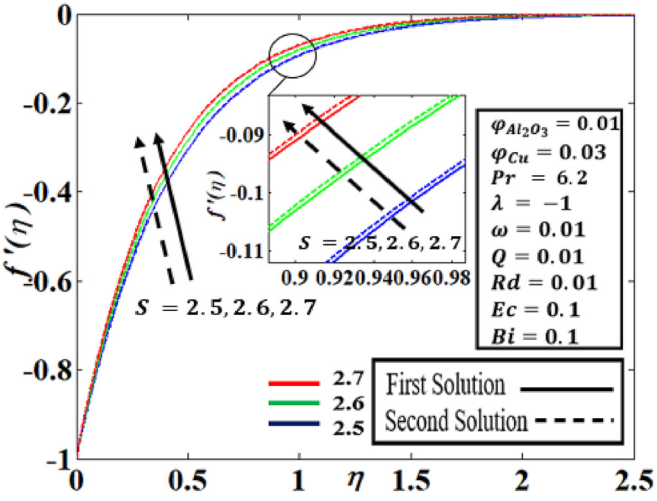


Fig. 11 $f\prime(\eta)$ profile for distinct S.

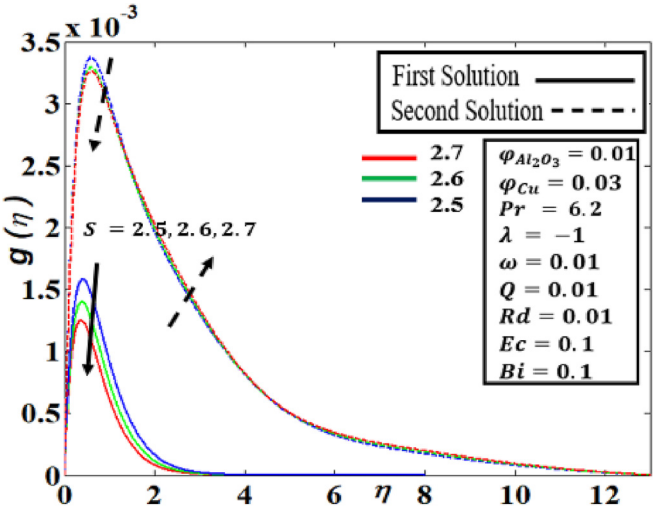


Fig. 12 $g(\eta)$ profile for distinct S.

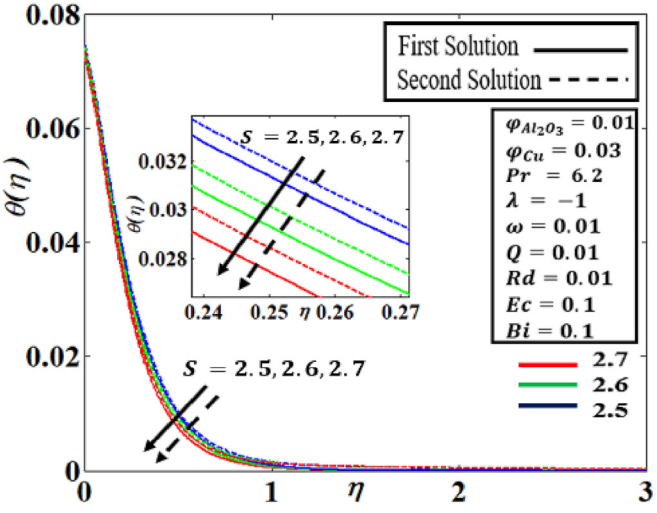


Fig. 13 $\theta(\eta)$ profile for distinct.S.

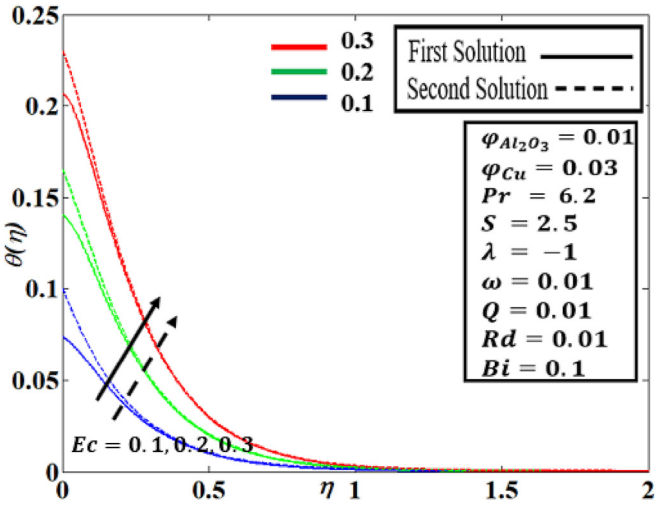


Fig. 14 $\theta(\eta)$ profile for distinct *Ec*.

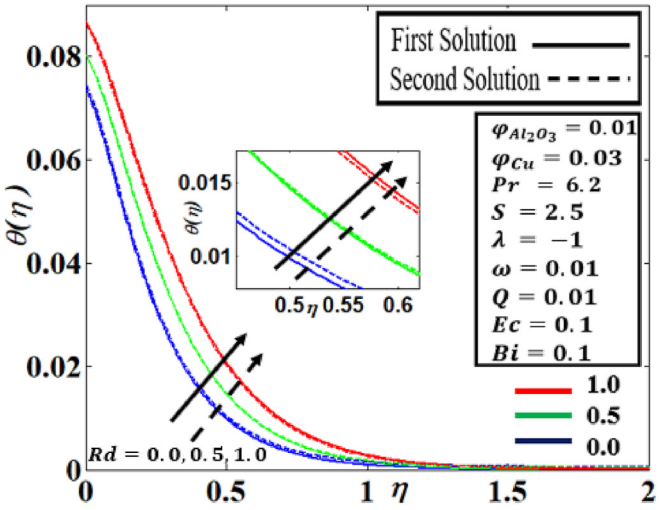


Fig. 15 $\theta(\eta)$ profile for different *Rd*.

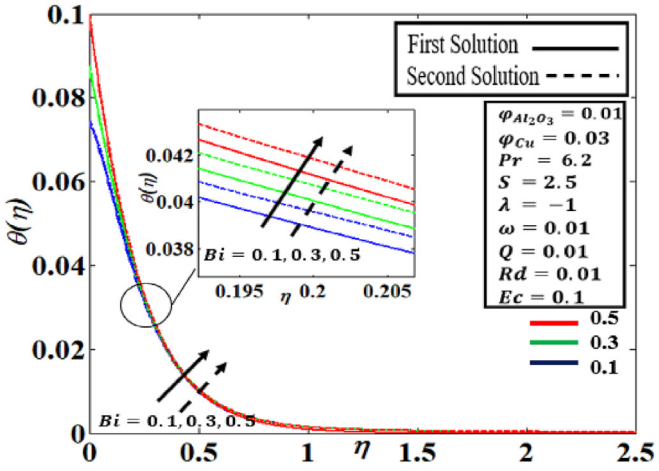


Fig. 16 $\theta(\eta)$ profile for distinct.*Bi*.

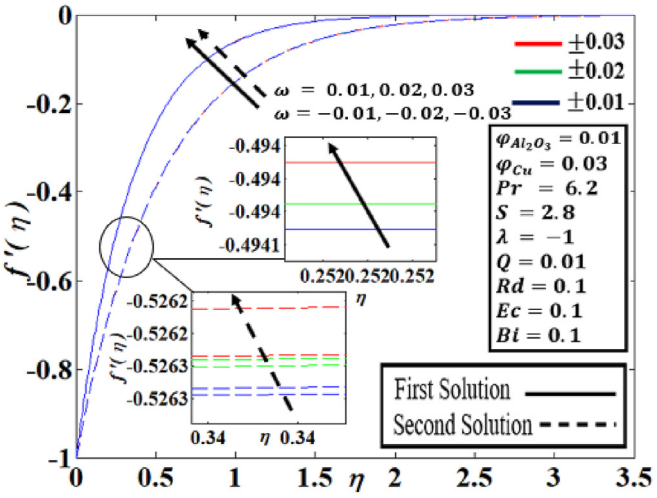


Fig. 17 $f\prime(\eta)$ profile for distinctω.

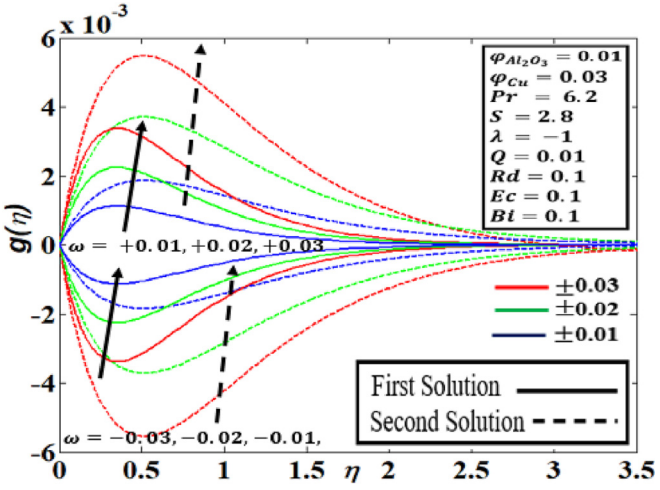


Fig. 18 $g(\eta)$ profile for distinct.ω.

Table 3 The comparison findings of ω at various values are when $\varphi_{Al_2O_3} = \varphi_{Cu} = S = Q = Rd = Ec = Bi = 0$, $\lambda = 1$, and $Pr = 6.2$.

	Nazar et al. [65]		Mustafa et al. [66]		Present findings	
ω	$f\prime\prime(0)$	$g\prime(0)$	$f\prime\prime(0)$	$g\prime(0)$	$f\prime\prime(0)$	$g\prime(0)$
0	−1	0	−1	0	−1	0
0.5	−1.1384	−0.5128	−1.13838	−0.51276	−1.138374	−0.512760
1.0	−1.3250	−0.8371	−1.32503	−0.83709	−1.325028	−0.837098
1.5	–	–	–	–	−1.496403	−1.082978
2.0	−1.6523	−1.2873	−1.65235	−1.28726	−1.652352	−1.287258
2.5	–	–	–	–	−1.795728	−1.465217
3.0	–	–	–	–	−1.928931	−1.624735
4.0	–	–	–	–	−2.171593	−1.905392
5.0	–	–	–	–	−2.390139	−2.150526

synergistic action. Moreover, when the effect of φ_{Cu} improved, the comportment of $g'(0)$declined in the first, and an upsurge in the second solution is noted in Fig. 6. From, Fig. 7 confirms that as φ_{Cu} is enhanced, the strength of $-\theta\prime(0)$ drops in both solutions. Boosting the quantity of φ_{Cu} can allow the boundary layer separation to happen at a later time, which is one of the physical validations of this declaration. Anuar et al. [35] reached comparable conclusions with their research.

Figs. 8-10 depict the following different values of $\varphi_{Cu} = 0.03, 0.05$,and 0.07 for the velocities and temperature profiles $(f'(\eta), g(\eta))$ and $\theta(\eta)$ respectively depending on a variety of factors including $\varphi_{Al_2O_3} = 0.01, Pr = 6.2, S = 2.5, \lambda = -1, \omega = Q = Rd = 0.01, Ec = 0.1$and $Bi = 0.1$ against η. Figs. 8 and 10 illustrate that, $f'(\eta)$ and $\theta(\eta)$ profiles rise, as well as an upsurge quantity of φ_{Cu} in both solutions. Furthermore, Fig. 9 reveals that $g(\eta)$ profile decreased in the first and enhanced in the second solution, but the reverse tendency can be seen caused by synergistic effects when $\eta > 4$ as the value φ_{Cu} improved. The progressive accumulation of φ_{Cu} physically allows the nanoparticles to travel quickly and causes the velocity to increase. Furthermore, a higher volume fraction of φ_{Cu} would give better thermal conductivity, enabling the temperature to rise. Consequently, a lesser solid volume fraction is required to accelerate cooling, while a greater solid volume fraction is obligatory to improve thermal. Anuar et al. [35] and Khashi et al. [60] noticed similar findings for temperature profiles.

The graphical representations of velocities $(f'(\eta), g(\eta))$ profiles and profile of temperature $\theta(\eta)$ under specific factor, which are $\varphi_{Al_2O_3} = 0.01, \varphi_{Cu} = 0.03, Pr = 6.2, \lambda = -1, \omega = Q = Rd = 0.01, Ec = 0.1$and $Bi = 0.1$ against suction parameter $S = 2.5, 2.6$,and 2.7 are portrayed in Figs. 11-13, respectively. Yan et al. [68] claimed that the values taken for Sin Figs. 11–13 should be between 2.25 and 3.0, so this is the range that was used, and this range $S \in [2.5 - 2.7]$ satisfied the boundary condition. From Fig. 11, the velocity $f'(\eta)$upsurged in both the first and second solutions as enhanced the quantity of suction S. From Fig. 12, the $g(\eta)$ profile in both solutions declined, but the second solution raised after $\eta > 2$ when growing the quantity of suction S effect. Besides, the temperature profile in Fig. 13 is reduced in both solutions as enhanced the amount of suction parameter S. Physically this is because suction exerts a drag force, which slows the flow of the hybrid nanofluid and functions as a factor that causes the flow to be slowed down. Additionally, it is because the boundary layer thickness is retarded.

Fig. 14 displays the amount of viscous dissipation $Ec = 0.1, 0.2$, and 0.3 at different aspects of a parameter, such as $\varphi_{Al_2O_3} = 0.01, \varphi_{Cu} = 0.03, Pr = 6.2, S = 2.5, \lambda = -1, \omega = Q = Rd = 0.01$, and $Bi = 0.1$ with respect to η for the temperature profile $\theta(\eta)$. As Yan et al. [68] employed a range of Ec $(0 \leq Ec \leq 0.6)$ in their investigation, and this assortment $(0.1 \leq Ec \leq 0.3)$ is used in Fig. 14, which satisfied the boundary conditions. Only Equation (12) contains an occurrence of the viscous dissipation Ec. Because the equations defining viscous dissipation Ec are unrelated to the equations expressing momentum (10) and (11), the quantity of viscous dissipation Ecdoes not impact the velocities profile. As a result, the viscous dissipation $Ec$is unaffected by the velocities profile. The $\theta(\eta)$ in both the first and second solutions enhanced as the quantities of viscous dissipation Ec upsurged. The physical description for this is that the viscosity of the fluid can absorb more energy as Ec rises, transform it into internal energy, and as a result, strengthen the temperature profile. Therefore, the strength of the heat transport rate increased due to the rate of viscous dissipation Ec grows. The same effect was observed in the temperature profile for viscous dissipation by Zainal et al. [52].

Fig. 15 demonstrates the different quantity of thermal radiation $Rd = 0.0, 0.5$,and 1.0 for $\theta(\eta)$ with $\varphi_{Al_2O_3} = 0.01$, $\varphi_{Cu} = 0.03, Pr = 6.2, S = 2.5, \lambda = -1, \omega = Q = 0.01, Ec = 0.1$ and $Bi = 0.1$ against η. Waini et al. [5] assumed a range of Rd $(0.0 \leq Rd \leq 2.0)$ in their analysis which falls in the set of ranges $(0.0 \leq Rd \leq 1.0)$, which is employed in Fig. 15 with satisfied the boundary conditions. The thermal radiation Rd only occurs in Equation (12). Consequently, the quantity of Rd does not affect the velocities profile, therefore, as a consequence of the fact that its equations are separate from those describing momentum Equations (10) and (11). Since the thickness of the thermal boundary layer increases continuously in the first and second solutions as the quantity of Rd intensifies. Physically, this indicates that higher Rdquantities lead to a lower temperature differential at the surface. The presence of a larger level of radiation results in the formation of a significant quantity of heat energy inside the system. The thermal radiation takes precedence over conduction with intensified Rd. As a result of the enhanced energy from radiation that exists in the flow field, the temperature $\theta(\eta)$ rises. Anuar et al. [35] found similar results.

Fig. 16 exhibits a plot of the temperature $\theta(\eta)$ profile of Biot parameter $Bi = 0.1, 0.3$,and 0.5 against η under several parameters such as $\varphi_{Al_2O_3} = 0.01, \varphi_{Cu} = 0.03, Pr = 6.2$, $S = 2.5, \lambda = -1, \omega = Q = Rd = 0.01$, and$Ec = 0.1$. Aly and Pop [59] applied a Bi range of $(0.1 \leq Bi \leq 1.0)$ in their research, which occurs inside the set of ranges $(0.1 \leq Bi \leq 0.5)$, which is used in Fig. 16 and meets the boundary requirements. Biot parameter Bi factor has no effect on the velocity $(f'(\eta), g(\eta))$ profiles, however, only the temperature $\theta(\eta)$ profile is needed for this investigation. It should be mentioned that when upsurged the value of Biot parameter Bi, the temperature $\theta(\eta)$ profile of both solutions is intensified. Physically, the Biot number and surface heat transfer rate are directly related (see Equation (13)), while the convective heating mechanism controls the surface temperature. When the Biot number rises, the surface's heat resistance falls dramatically. Therefore, when the Biot parameter Bi increases, the amount of surface heat transfer correspondingly enhances. Aly and Pop [59] observed comparable outcomes.

The velocity $(f'(\eta), g(\eta))$ profiles of positive and negative rotational parameter $\omega = \pm 0.01, \pm 0.02$, and ± 0.03 are shown in Figs. 17-18, with the occurrence of definite parameters such as $\varphi_{Al_2O_3} = 0.01, \varphi_{Cu} = 0.03, Pr = 6.2, S = 2.8, \lambda = -1, Q = 0.01, Rd = Ec = 0.1$, and$Bi = 0.1$. The quantities of $\omega = 0.01, 0.02$, and 0.03 in Figs. 17-18 are the same as those in Anuar et al. [35]. In Fig. 17, we can see the velocity $f'(\eta)$ profile both solutions increased when enhanced the positive rotational parameter ω however, no oscillation effect on velocity $f'(\eta)$ when improved the negative rotational ω parameter. In Fig. 18, when both positive and negative rotational parameter ω are augmented, the behaviour of the $g(\eta)$ profile demonstrates dual, and both solutions intensified. The angular thickness of the momentum boundary layer improved as the rotational parameter's value increased. This suggests that the fluid problem with the hybrid nanofluids has an approach that is symmetrical. Physically, the nanoparticles move rapidly, which contributes to the enhancement of the velocity of the hybrid nanofluid flow. Lund et al. [67] found a comparable result for the rotational parameter.

5. Conclusion

This research was inspired by the fact that hybrid nanofluids can be tailored to suit specific applications by varying the type and concentration of nanoparticles in the base fluid. This versatility makes them suitable for a wide range of applications, including electronics cooling, solar thermal energy conversion, and biomedical applications. By applying the Bvp4c numerical process in the Matlab software, the influence of convective boundary condition, radiation, heat source/sink, and viscous dissipation on a 3-D hybrid nanofluid flow including a rotating stretching/shrinking surface has been explored. This research focuses on the behaviour of $f\prime\prime(0)$, $g\prime(0)$, $-\theta\prime(0)$, $f'(\eta), g(\eta)$ and $\theta(\eta)$ under the influence of solid volume fraction copper, suction/injection, viscous dissipation, convective boundary condition and rotational parameter on hybrid nanofluid flow. The following is an outline of the major conclusions from this study:

i. The results of Equations (2–4) are non-unique, while $\lambda \geq \lambda_{ci}$ for shrinking sheet and $S \geq S_{ci}$ for suction effect.
ii. Intensification in the solid volume fraction φ_{Cu} enhances the reduced skin friction $f''(0)$ in both solutions but declines in the first and upsurges in the second solutions in $g\prime(0)$ for suction effect.
iii. Reduced skin friction $f''(0)$ upsurges in the first solution and declines in the second solution, but an opposite tendency is noticed in $g\prime(0)$ when there is an increase in the solid volume fraction φ_{Cu} for the shrinking sheet.
iv. The $-\theta\prime(0)$ falls in both solutions, while the volume fraction of copper improved for both shrinking and suction effects.
v. The velocity $f'(\eta)$ profile upsurges in both solutions when copper's volume fraction and suction parameter are enhanced.
vi. The $g(\eta)$ profile declined in the first solution and improved in the second solution, but the opposite tendency can be noticed due to when $\eta > 4$ as the value φ_{Cu} upsurged.
vii. Thermal boundary layer thickness upsurges as the quantity of solid volume fraction of copper, viscous dissipation, radiation, and Biot number are enhanced.
viii. Thermal boundary layer thickness declines when augmented the value of the suction effect.
ix. Both solutions are increased in velocity $f'(\eta)$ profile and $g(\eta)$ profile when the increment of positive and negative rotational parameter ω.

Funding

"Project financed by Lucian Blaga University of Sibiu through research grant LBUS-IRG-2022-08".

Declaration of Competing Interest

The authors declare that they have no known competing financial interests or personal relationships that could have appeared to influence the work reported in this paper.

Acknowledgement

The authors extend their appreciation to the Deanship of Scientific Research at King Khalid University Abha 61421, Asir, Kingdom of Saudi Arabia for funding this work through the Large Groups Project under grant number RGP.2/142/44.

References

[1] J. Buongiorno, Convective transport in nanofluids, J. Heat Transfer 128 (3) (2006) 240–250.
[2] R.K. Tiwari, M.K. Das, Heat transfer augmentation in a two-sided lid-driven differentially heated square cavity utilizing nanofluids, Int. J. Heat Mass Transf. 50 (9–10) (2007) 2002–2018.
[3] S.A. Devi, S.S.U. Devi, Numerical investigation of hydromagnetic hybrid Cu–Al2O3/water nanofluid flow over a permeable stretching sheet with suction, International Journal of Nonlinear Sciences and Numerical Simulation 17 (5) (2016) 249–257.
[4] A. Asghar, A.F. Chandio, Z. Shah, N. Vrinceanu, W. Deebani, M. Shutaywi, L.A. Lund, Magnetized mixed convection hybrid nanofluid with effect of heat generation/absorption and velocity slip condition, Heliyon 9 (2) (2023) e13189.
[5] I. Waini, A. Ishak, I. Pop, Hybrid nanofluid flow and heat transfer over a nonlinear permeable stretching/shrinking surface, Int. J. Numer. Meth. Heat Fluid Flow (2019).
[6] I. Waini, A. Ishak, I. Pop, Transpiration effects on hybrid nanofluid flow and heat transfer over a stretching/shrinking sheet with uniform shear flow, Alex. Eng. J. 59 (1) (2020) 91–99.
[7] M. Behrouz, S. Dinarvand, M.E. Yazdi, H. Tamim, I. Pop, A.J. Chamkha, Mass-based hybridity model for thermomicropolar binary nanofluid flow: first derivation of angular momentum equation, Chin. J. Phys. (2023).
[8] S. Dinarvand, M.N. Rostami, Three-dimensional squeezed flow of aqueous magnetite–graphene oxide hybrid nanofluid: a novel hybridity model with analysis of shape factor effects, Proceedings of the Institution of Mechanical Engineers, Part E: Journal of Process Mechanical Engineering 234 (2) (2020) 193–205.
[9] M. Izady, S. Dinarvand, I. Pop, A.J. Chamkha, Flow of aqueous Fe2O3–CuO hybrid nanofluid over a permeable stretching/shrinking wedge: A development on Falkner-Skan problem, Chin. J. Phys. 74 (2021) 406–420.
[10] S. Dinarvand, H. Berrehal, I. Pop, A.J. Chamkha, Blood-based hybrid nanofluid flow through converging/diverging channel with multiple slips effect: a development of Jeffery-Hamel problem, Int. J. Numer. Meth. Heat Fluid Flow 33 (3) (2023) 1144–1160.
[11] S. Dinarvand, S.M. Mousavi, M. Yousefi, M. Nademi Rostami, MHD flow of MgO-Ag/water hybrid nanofluid past a moving slim needle considering dual solutions: An applicable model for hot-wire anemometer analysis, Int. J. Numer. Meth. Heat Fluid Flow 32 (2) (2022) 488–510.
[12] A. Asghar, T.Y. Ying, K. Zaimi, Two-dimensional magnetized mixed convection hybrid nanofluid over a vertical exponentially shrinking sheet by thermal radiation, joule heating, velocity and thermal slip conditions, Journal of Advanced Research in Fluid Mechanics and Thermal Sciences 95 (2) (2022) 159–179.
[13] N. Abbas, W. Shatanawi, A.M. Taqi, Thermodynamic study of radiative chemically reactive flow of induced MHD sutterby nanofluid over a nonlinear stretching cylinder, Alex. Eng. J. 70 (2023) 179–189.
[14] W. Shatanawi, N. Abbas, T.A. Shatnawi, F. Hasan, Heat and mass transfer of generalized fourier and Fick's law for second-

grade fluid flow at slendering vertical Riga sheet, Heliyon 9 (3) (2023).
[15] S. Nadeem, M.N. Khan, N. Abbas, Transportation of slip effects on nanomaterial micropolar fluid flow over exponentially stretching, Alex. Eng. J. 59 (5) (2020) 3443–3450.
[16] M. Amjad, I. Zehra, S. Nadeem, N. Abbas, A. Saleem, A. Issakhov, Influence of Lorentz force and induced magnetic field effects on Casson micropolar nanofluid flow over a permeable curved stretching/shrinking surface under the stagnation region, Surf. Interfaces 21 (2020) 100766.
[17] A. Asghar, T.Y. Ying, W.M.K.A.W. Zaimi, Two-Dimensional Mixed Convection and Radiative Al2O3-Cu/H2O Hybrid Nanofluid Flow over a Vertical Exponentially Shrinking Sheet with Partial Slip Conditions, CFD Lett. 14 (3) (2022) 22–38.
[18] P. Nanda, N. Sandeep, C. Sulochana, G.P. Ashwinkumar, Enhanced heat transmission in methanol-based AA7072/AA7075 tangent hyperbolic hybrid nanofluid flow along a nonlinear expandable surface, Numerical Heat Transfer, Part A: Applications 83 (7) (2023) 711–725.
[19] N. Sandeep, C. Sulochana, G.P. Ashwinkumar, Understanding the dynamics of chemically reactive Casson liquid flow above a convectively heated curved expanse, Proc. Inst. Mech. Eng. C J. Mech. Eng. Sci. 236 (24) (2022) 11420–11430.
[20] K. Anantha Kumar, N. Sandeep, S.P. Samrat, G.P. Ashwinkumar, Effect of electromagnetic induction on the heat transmission in engine oil-based hybrid nano and ferrofluids: A nanotechnology application, Proceedings of the Institution of Mechanical Engineers, Part E: Journal of Process Mechanical Engineering 09544089221139569 (2022).
[21] N. Sandeep, P. Nanda, G.P. Ashwinkumar, Transpiration effect on Falkner-Skan bioconvective mixed nanoliquid flow above a poignant wedge, Proc. Inst. Mech. Eng. C J. Mech. Eng. Sci. 237 (8) (2023) 1793–1805.
[22] S.P. Samrat, Y.H. Gangadharaiah, G.P. Ashwinkumar, N. Sandeep, Effect of exponential heat source on parabolic flow of three different non-Newtonian fluids, Proceedings of the Institution of Mechanical Engineers, Part E: Journal of Process Mechanical Engineering 236 (5) (2022) 2131–2138.
[23] G.P. Ashwinkumar, M. Girinath Reddy, N. Sandeep, Convective heat transfer in MHD Cu-TiO2-H2O cross nanofluid flow over three diverse surfaces, Proceedings of the Institution of Mechanical Engineers, Part E: Journal of Process Mechanical Engineering 236 (5) (2022) 1800–1807.
[24] N. Sandeep, S.P. Samrat, G.P. Ashwinkumar, Flow and heat transfer in radiative MHD dusty-hybrid ferrofluids, Waves Random Complex Media (2022) 1–14.
[25] M. Sajjad, A. Mujtaba, A. Asghar, T.Y. Ying, Dual solutions of magnetohydrodynamics Al2O3 + Cu hybrid nanofluid over a vertical exponentially shrinking sheet by presences of joule heating and thermal slip condition, CFD Lett. 14 (8) (2022) 100–115.
[26] P.V. Satya Narayana, N. Tarakaramu, D. Harish Babu, Influence of chemical reaction on MHD couple stress nanoliquid flow over a bidirectional stretched sheet, Int. J. Ambient Energy 43 (1) (2022) 4928–4938.
[27] P.V. Satya Narayana, N. Tarakaramu, G. Sarojamma, I.L. Animasaun, Numerical simulation of nonlinear thermal radiation on the 3D flow of a couple stress Casson nanofluid due to a stretching sheet, J. Therm. Sci. Eng. Appl. 13 (2) (2021).
[28] K. Kumaraswamy Naidu, D. Harish Babu, S. Harinath Reddy, P.V. Satya Narayana, Radiation and partial slip effects on magnetohydrodynamic Jeffrey nanofluid containing gyrotactic microorganisms over a stretching surface, J. Therm. Sci. Eng. Appl. 13 (3) (2021).
[29] B. Venkateswarlu, P.V. Satya Narayana, Cu-Al2O3/H2O hybrid nanofluid flow past a porous stretching sheet due to temperatue-dependent viscosity and viscous dissipation, Heat Transfer 50 (1) (2021) 432–449.
[30] P.V. Satya Narayana, B. Venkateswarlu, S. Venkataramana, Thermal radiation and heat source effects on a MHD nanofluid past a vertical plate in a rotating system with porous medium. *Heat Transfer—Asian*, Research 44 (1) (2015) 1–19.
[31] F. Wang, N. Tarakaramu, N. Sivakumar, P.S. Narayana, D.H. Babu, S. Ramalingam, Three dimensional nanofluid motion with convective boundary condition in presents of nonlinear thermal radiation via stretching sheet, J. Indian Chem. Soc. 100887 (2023).
[32] N. Tarakaramu, P.V. Satya Narayana, N. Sivakumar, D. Harish Babu, K. Bhagya Lakshmi, Convective conditions on 3D magnetohydrodynamic (MHD) non-Newtonian nanofluid flow with nonlinear thermal radiation and heat absorption: a numerical analysis, Journal of Nanofluids 12 (2) (2023) 448–457.
[33] T. Hayat, S. Nadeem, Heat transfer enhancement with Ag–CuO/water hybrid nanofluid, Results Phys. 7 (2017) 2317–2324.
[34] T. Hayat, S. Nadeem, A.U. Khan, Rotating flow of Ag-CuO/H 2 O hybrid nanofluid with radiation and partial slip boundary effects, The European Physical Journal E 41 (6) (2018) 1–9.
[35] N.S. Anuar, N. Bachok, I. Pop, Radiative hybrid nanofluid flow past a rotating permeable stretching/shrinking sheet, Int. J. Numer. Meth. Heat Fluid Flow (2020).
[36] Y.Y. Teh, A. Asghar, Three Dimensional MHD Hybrid Nanofluid Flow with Rotating Stretching/Shrinking Sheet and Joule Heating, CFD Lett. 13 (8) (2021) 1–19.
[37] L.A. Lund, Z. Omar, I. Khan, Darcy-Forchheimer porous medium effect on rotating hybrid nanofluid on a linear shrinking/stretching sheet, Int. J. Numer. Meth. Heat Fluid Flow (2021).
[38] L.A. Lund, Z. Omar, I. Khan, E.S.M. Sherif, Dual branches of MHD three-dimensional rotating flow of hybrid nanofluid on nonlinear shrinking sheet, Computers, Materials and Continua 66 (1) (2020) 127–139.
[39] L. Kolsi, S. Dero, L.A. Lund, U.F. Alqsair, M. Omri, S.U. Khan, Thermal stability and performances of hybrid nanoparticles for convective heat transfer phenomenon with multiple solutions, Case Studies in Thermal Engineering 28 (2021) 101684.
[40] U. Khan, A. Shafiq, A. Zaib, D. Baleanu, Hybrid nanofluid on mixed convective radiative flow from an irregular variably thick moving surface with convex and concave effects, Case Studies in Thermal Engineering 21 (2020) 100660.
[41] P. Sreedevi, P.S. Reddy, A. Chamkha, Heat and mass transfer analysis of unsteady hybrid nanofluid flow over a stretching sheet with thermal radiation, SN Applied Sciences 2 (7) (2020) 1–15.
[42] Dero, S., Lund, L. A., Shah, Z., Bonyah, E., & Deebani, W. (2021). Numerical Analysis of Cu + Al 2 O 3/H 2 O Hybrid Nanofluid of Streamwise and Cross Flow with Thermal Radiation Effect: Duality and Stability. *Mathematical Problems in Engineering*, *2021*.
[43] N.C. Roşca, A.V. Roşca, I. Pop, Axisymmetric flow of hybrid nanofluid due to a permeable non-linearly stretching/shrinking sheet with radiation effect, Int. J. Numer. Meth. Heat Fluid Flow (2020).
[44] A. Asghar, L.A. Lund, Z. Shah, N. Vrinceanu, W. Deebani, M. Shutaywi, Effect of thermal radiation on three-dimensional magnetized rotating flow of a hybrid nanofluid, Nanomaterials 12 (9) (2022) 1566.
[45] M.R. Eid, M.A. Nafe, Thermal conductivity variation and heat generation effects on magneto-hybrid nanofluid flow in a porous medium with slip condition, Waves Random Complex Media (2020) 1–25.
[46] N.A. Zainal, R. Nazar, K. Naganthran, I. Pop, Heat generation/absorption effect on MHD flow of hybrid nanofluid over bidirectional exponential stretching/shrinking sheet, Chin. J. Phys. 69 (2021) 118–133.

[47] N.S. Wahid, Norihan Md Arifin, Najiyah Safwa Khashi'ie, and Ioan Pop. "Hybrid nanofluid slip flow over an exponentially stretching/shrinking permeable sheet with heat generation.", Mathematics 9 (1) (2020) 30.
[48] A. Jamaludin, K. Naganthran, R. Nazar, I. Pop, MHD mixed convection stagnation-point flow of Cu-Al2O3/water hybrid nanofluid over a permeable stretching/shrinking surface with heat source/sink, European Journal of Mechanics-B/Fluids 84 (2020) 71–80.
[49] M.N. Othman, A. Jedi, N.A.A. Bakar, MHD flow and heat transfer of hybrid nanofluid over an exponentially shrinking surface with heat source/sink, Appl. Sci. 11 (17) (2021) 8199.
[50] P.M. Kishore, D. Bhanumathi, V.S. Verma, The influence of chemical reaction and viscous dissipation on unsteady MHD free convection flow past an exponentially accelerated vertical plate with variable surface conditions, Chemical Industry and Chemical Engineering Quarterly/CICEQ 19 (2) (2013) 181–193.
[51] B. Gebhart, Effects of viscous dissipation in natural convection, J. Fluid Mech. 14 (2) (1962) 225–232.
[52] N.A. Zainal, R. Nazar, K. Naganthran, I. Pop, Viscous dissipation and MHD hybrid nanofluid flow towards an exponentially stretching/shrinking surface, Neural Comput. & Applic. 33 (17) (2021) 11285–11295.
[53] Syahirah Wahid, N., Md Arifin, N., Safwa Khashi'ie, N., Pop, I., Bachok, N., & Ezad Hafidz Hafidzuddin, M. (2022). Three-Dimensional Stretching/Shrinking Flow of Hybrid Nanofluid with Slips and Joule Heating. *Journal of Thermophysics and Heat Transfer*, 1-10.
[54] L.A. Lund, Z. Omar, J. Raza, I. Khan, Magnetohydrodynamic flow of Cu–Fe3O4/H2O hybrid nanofluid with effect of viscous dissipation: dual similarity solutions, J. Therm. Anal. Calorim. 143 (2) (2021) 915–927.
[55] I. Waini, A. Ishak, I. Pop, Radiative and magnetohydrodynamic micropolar hybrid nanofluid flow over a shrinking sheet with Joule heating and viscous dissipation effects, Neural Comput. & Applic. 34 (5) (2022) 3783–3794.
[56] H.M. Sayed, E.H. Aly, K. Vajravelu, Influence of slip and convective boundary conditions on peristaltic transport of non-Newtonian nanofluids in an inclined asymmetric channel, Alex. Eng. J. 55 (3) (2016) 2209–2220.
[57] A. Aziz, A similarity solution for laminar thermal boundary layer over a flat plate with a convective surface boundary condition, Commun. Nonlinear Sci. Numer. Simul. 14 (4) (2009) 1064–1068.
[58] S.S.U. Devi, S.A. Devi, Numerical investigation of three-dimensional hybrid Cu–Al2O3/water nanofluid flow over a stretching sheet with effecting Lorentz force subject to Newtonian heating, Can. J. Phys. 94 (5) (2016) 490–496.
[59] E.H. Aly, I. Pop, MHD flow and heat transfer over a permeable stretching/shrinking sheet in a hybrid nanofluid with a convective boundary condition, Int. J. Numer. Meth. Heat Fluid Flow (2019).
[60] N.S. Khashi'ie, N.M. Arifin, I. Pop, R. Nazar, E.H. Hafidzuddin, N. Wahi, Three-dimensional hybrid nanofluid flow and heat transfer past a permeable stretching/shrinking sheet with velocity slip and convective condition, Chin. J. Phys. 66 (2020) 157–171.
[61] W.F. Xia, S. Ahmad, M.N. Khan, H. Ahmad, A. Rehman, J. Baili, T.N. Gia, Heat and mass transfer analysis of nonlinear mixed convective hybrid nanofluid flow with multiple slip boundary conditions, Case Studies in Thermal Engineering 32 (2022) 101893.
[62] Waini, I., Ishak, A., & Pop, I. (2019). Hybrid nanofluid flow and heat transfer past a permeable stretching/shrinking surface with a convective boundary condition. In *Journal of Physics: Conference Series* (Vol. 1366, No. 1, p. 012022). IOP Publishing.
[63] R. Jusoh, K. Naganthran, A. Jamaludin, M.H. Ariff, M.F.M. Basir, I. Pop, Mathematical analysis of the flow and heat transfer of Ag-Cu hybrid nanofluid over a stretching/shrinking surface with convective boundary condition and viscous dissipation, Data Analytics and Applied Mathematics (DAAM) 1 (1) (2020) 11–22.
[64] N. Hale, D.R. Moore, A sixth-order extension to the Matlab package Bvp4c of J, Kierzenka and L, Shampine, 2008.
[65] R. Nazar, N. Amin, I. Pop, Unsteady boundary layer flow due to a stretching surface in a rotating fluid, Mech. Res. Commun. 31 (1) (2004) 121–128.
[66] M. Mustafa, A. Mushtaq, T. Hayat, A. Alsaedi, Rotating flow of magnetite-water nanofluid over a stretching surface inspired by nonlinear thermal radiation, PLoS One 11 (2) (2016) e0149304.
[67] L.A. Lund, Z. Omar, S. Dero, D. Baleanu, I. Khan, Rotating 3D flow of hybrid nanofluid on exponentially shrinking sheet: Symmetrical solution and duality, Symmetry 12 (10) (2020) 1637.
[68] L. Yan, S. Dero, I. Khan, I.A. Mari, D. Baleanu, K.S. Nisar, H. S. Abdo, Dual solutions and stability analysis of magnetized hybrid nanofluid with joule heating and multiple slip conditions, Processes 8 (3) (2020) 332.